Simple flow models of accretionary prisms: predictions for coexisting arc-normal compression and extension, and implications for locked zones on the interplate megathrust

Y. Furukawa

Division of Earth and Planetary Sciences, Graduate School of Science, Kyoto University

Sakyo-ku, Kyoto 606-8502, Japan

Tel./Fax.: 075-753-3910/075-753-3717

Abstract

In accretionary prisms formed in subduction zones, accreted sediments deform due to the drag of the subducting plate, resulting in arc-normal compression. In the Cascadia and eastern Nankai subduction zones, however, arc-parallel normal faults, which indicate the occurrence of arc-normal extension, have been observed at the rear of the accretionary prisms. In this study, the deformation caused by the subducting plate in the accretionary prism is calculated using a simple fluid model that considers temperature-dependent rheology. The qualitative results show that a circulating flow is induced by the subducting plate under a lid formed at the rear of the accretionary prisms at higher temperatures, while, in lower-temperature prisms, the flow pattern is analogous to a simple corner flow, and the circulating flow is not induced. Prism materials flow trenchward just under the lid, and this return flow may be the cause of the arc-normal extension observed in the accretionary prisms. Most of the subduction velocity is accommodated by ductile deformation at the rear of the accretionary prisms, resulting in lower seismic coupling at the deeper interplate megathrusts. In the frontal part of the accretionary prisms, where imbricate thrusts develop, low rigidity due to high porosity and pore fluid pressure in the compacting sediment, together with higher concentrations of clay minerals with low frictional coefficients, probably prevents seismic slip at the interplate megathrusts. Locked zones develop between the extensional and imbricate thrust regions in the subduction zones. For low-temperature prisms, locked zones are located arcside of the imbricate thrust region. The fore-arc basin is thus formed above the locked zone in accretionary prisms. In the eastern Nankai subduction zone, another locked zone is estimated to be located in the lower crust. The location of the arc side of the imbricate

thrust region in the western and central Nankai subduction zones may be controlled by the thrust intersection with the top of the lower crust and the splay-fault, respectively.

Introduction

In most subduction zones, subducting sediments accrete to the overlying plate to form accretionary prisms (von Huene and Scholl, 1991). Offshore seismic reflection studies have revealed that sediments on the subducting plate are stripped off and accreted to the overlying plate in arcward-dipping imbricate thrust packets (Karig and Sharman III, 1975). The accretionary prism is considered to be mechanically analogous to a wedge of sand in front of a moving bulldozer; the sand deforms internally until it reaches a stable configuration, where gravitational forces balance the drag exerted by the subducting plate (Davis et al., 1983). The taper of the accretionary prism can be predicted by this critical taper model.

Analog models for the growth of the accretionary prism due to incoming sediments at the trench show that the trajectory of accreted materials is like that of a corner flow of a viscous fluid with a moving bottom boundary (Cowan and Silling, 1978). The macroscopic shape and temperature structure of the accretionary prism have been estimated using viscous corner flow models (Dahlen and Barr, 1989; Emerman and Turcotte, 1983; Furukawa, 1999; Platt, 2000).

These models show that arc-normal compressional stress is dominant in the accretionary prism (Davis et al., 1983; Liu and Ranalli, 1998). In the Cascadia and Nankai subduction zones, however, arc-parallel normal faults have been observed at the rear of the accretionary prisms (Arai et al., 2006; McNeill et al., 1997), indicating arc-normal extension; in contrast,

imbricate thrusts develop at the front of the accretionary prism under arc-normal compressional stress (Nakanishi et al., 1998; Booth-Rea et al., 2008).

In both these subduction zones, arc-normal compression at the front and extension at the rear of the accretionary prisms coexist. Platt (1986) suggested that the arc-normal extension may be caused by uplift due to basal accretion at the rear of the accretionary prism, but there is no evidence to confirm the occurrence of active uplift in the Quaternary for these accretionary prisms (McNeill et al., 2000; Yamaji et al., 2003).

In this study, the temperature and deformation in these accretionary prisms are calculated using a simple viscous fluid model that considers temperature-dependent viscosity, and a qualitative model is presented, in which arc-normal extension and compression coexist. The deformation in the accretionary prisms affects the strain accumulation in the overlying plate caused by basal drag of the subducting plate, and the model results are used to estimate the distribution of locked zones at the interplate megathrusts in subduction zones including Cascade and Southwest Japan.

Regional Setting

Cascadia

In the Cascadia subduction zone off Washington and the northern Oregon, the relatively young Juan de Fuca plate is subducting under the North American plate, and the accretionary prism has widened to more than 100 km. Reflection seismic surveys have revealed the existence of active extensional structures on the upper slope and shelf in this accretionary prism (Fig. 1), whereas imbricate thrusts have been observed on the lower slope, indicating

arc-normal shortening (Booth-Rea et al., 2008; McNeill et al., 1997). In the middle of the prism, there is an active out-of-sequence thrust named the Cascadia main thrust (CMT), which is the seaward limit of the upper slope and shows displacements larger than that of the underlying thrusts (Booth-Rea et al., 2008). The lower slope between the CMT and the deformation front has very small tilts (<1°). The lower slope can mainly be divided into two domains, which are characterized by landward-vergent imbricate thrusts and folds without faults, arcward from the deformation front (Booth-Rea et al., 2008).

The normal faults in the extensional region have arc-parallel strikes, indicating arc-normal extension. In the extensional region, landward-vergent, listric normal faults are dominant (Booth-Rea et al., 2008). Reflection seismic profiles show that the well-stratified layer in which the normal faults can be traced has a seismically opaque layer beneath. Stratigraphy results using outcrops and borehole data show that a chaotic and highly sheared formation from the Eocene to middle Miocene that is named the Mélange and Broken Formation (MBF) underlies younger stratified sediments; the opaque layer probably corresponds to the highly shared MBF (McNeill et al., 2000). The seaward stretch of the MBF is suggested to be the cause of the arc-normal extension in this region (McNeill et al., 2000).

In this extensional region, the accretionary prism is suggested to be composed of accreted sediments from the middle Eocene and younger, which were thrust under the Crescend/Siletz mafic terrane in the Paleocene and early Eocene (Tréhu et al., 1994). In this region, the estimated western border of the mafic terrane warps around the Olympic Mountains and is located landward of the coast, as shown in Fig. 1 (McNeill et al., 1997;

Tréhu et al., 1994). Seismic surveys have shown that the accreted sediment is thicker and reaches the surface of the subducting Juan de Fuca plate at a depth of 20–30 km under the Olympic Mountains (Parsons et al., 1999; Ramachandran et al., 2006). The extensional structure is observed off the region where the mafic terrane is located landward of the coast.

Southwest Japan

In southwest Japan, the Philippine Sea plate is subducting at the Nankai trough under the Eurasian plate, and a large accretionary prism of more than 100 km in width has been formed. In the eastern Nankai subduction zone off the Tokai area, reflection seismic profiles have shown that there are normal faults with strikes in the arc-parallel direction on the continental shelf and the upper slope of the accretionary prism (Arai et al., 2006). Normal faults have also been observed onshore in this region (Yamaji et al., 2003), as shown in Fig. 2. Most of the faults are landward-dipping, and sediments are deposited in a half-graben structure formed by the fault displacements. The Ensyu thrust system (ETS) is located between the forearc basin and extensional region and is the seaward limit of the upper slope (Fig. 2). In the frontal part of the accretionary prism off the Tokai area, imbricate thrusts are well developed and the outer ridge can be easily traced from the bathymetry (Nakanishi et al., 1998).

In this area, the depth extent of the felsic sediment layer riding on the subducting plate has not been well estimated. Reflection seismic profiles for the accretionary prism off the Tokai area show that the accreted sediment appears to extend to a depth of more than 20 km on the subducting Philippine Sea plate (Kodaira et al., 2003; Nakanishi et al., 1998). In the central Nankai subduction zone off the Kii peninsula, the felsic layer extends to a depth of

~25 km on the subducting plate in the estimated seismic structures (Hirose and Ito, 2007), assuming that the P-wave velocity of silicic rocks in this area is less than 6.4 km/s (Nakanishi et al., 2002). In southwest Japan, the Median Tectonic Line (MTL) runs in the arc-parallel direction; it is one of the longest and most active fault systems in Japan and is the boundary between the high-T and high-P metamorphic terranes.

In the western and central Nankai subduction zones off the Shikoku Island and Kii peninsula, respectively, an extensional structure is not observed for the shelf and upper slope. The estimated seismic velocity structures for the crust in the southwest Japan show that the thickness of the felsic accretionary prism on top of the descending Philippine Sea plate increases eastward. In the western Nankai subduction zone, the depth extent of the accretionary prism is less than 15 km (Kodaira et al., 2000; Takahashi et al., 2002). In the central zone off the Kii peninsula, the accreted material appears to reach a depth of 20–25 km on the subducting plate (Hirose and Ito, 2007; Nakanishi et al., 2008).

In the central Nankai accretionary prism off the Kii peninsula, the forearc basin becomes wider, and the outer ridge is located far seaward of the intersection between the megathrust and top of the lower crust (Hirose and Ito, 2007; Nakanishi et al., 2002). Reflection seismic studies have shown that there is an out-of-sequence splay-fault branching from the megathrust at a depth of 10 km that breaks the overlying crust (Park et al., 2002). The surface trace of this fault is located seaward along the outer ridge as shown in Fig. 2. This splay-fault is a fundamental structure in the central Nankai subduction zone; the frontal accretion of sediments by the addition of thrust packets mainly occurs seaward of the splay-fault, and the outer ridge is formed above the hanging wall of this splay-fault (Moore et al., 2007). In the

region arcward of the splay-fault, internal deformation of the accretionary prism, then, decreases, and the forearc basin is formed there. In this area, the splay-fault acts as a backstop for the frontal accretion of incoming sediments.

Model

A simple 2-D numerical model is used to calculate temperature and deformation in the accretionary prism in this study (Furukawa, 1993; Furukawa, 1999). The model configuration is shown in Fig. 3. Rigid oceanic plate subducts under an accretionary prism, and viscous flow is induced due to basal shear caused by the subducting plate. The upper and lower crusts are assumed to be composed of felsic and mafic crystalline rocks, respectively; they are also assumed to have the high shear strength compared to sediments in the accretionary prism. In this model, the accretionary prism has a flat surface; accreted material near the base of the prism is dragged down deeper and the subsidence caused by the downward flow at the front of the prism is filled with incoming sediments. At the rear of the accretionary prism, the surface becomes upheaved due to the addition of accreted sediments that are carried deep into the prism by the downward flow, which results in erosion of the upheaved surface.

For 2-D viscous flow of an incompressible fluid, the momentum equation is expressed in the Cartesian coordinate system using a stream function (Ψ) as

$$\left(\frac{\partial^2}{\partial x^2}-\frac{\partial^2}{\partial z^2}\right)\left[\eta\left(\frac{\partial^2}{\partial x^2}-\frac{\partial^2}{\partial z^2}\right)\Psi\right]+4\frac{\partial^2}{\partial x\partial z}\left(\eta\frac{\partial^2\Psi}{\partial x\partial z}\right)=0\,,$$

where η and z denote the viscosity and depth.

To estimate the temperature structure in the prism, radiogenic heat generation, strain

heating, and frictional heating at the plate interface are considered. The energy equation is then expressed as

$$\frac{\partial T}{\partial t} + u \cdot \nabla T = \kappa \nabla^2 T + H + \eta (\nabla u)^2 + \tau u',$$

where T, t, u, κ, η, H, u' and τ are the temperature, time, flow velocity, thermal diffusivity, viscosity, radiogenic heat generation, velocity difference at the plate boundary, and shear stress, respectively.

Shear-stress-free and fixed boundary conditions are set for the top and the landward boundaries of the accretionary prism, respectively. The temperature at the top boundary is set to 0°C. At the seaward boundary, an oceanic geotherm calculated using the simple half space cooling model (Parsons and Sclater, 1977) is applied that is estimated from the age of the subducting oceanic plate. At the landward boundary, a 1-D steady state geotherm is calculated using observed values of surface heat flow and crustal heat generation (Lachenbruch, 1970). At the bottom boundary of the model (Fig. 3), isotherms are set parallel to the upper surface of the subducting plate. In this model, thermal diffusivity is set to $0.8 \cdot 10^{-6}$ m^2/s; thermal conductivity and radiogenic heat generation values are listed in Table 1 (Furukawa, 1995; Wang et al., 1995).

Assuming that the accretionary prism deforms macroscopically like the corner flow of a viscous fluid, the apparent bulk viscosity of the accretionary prism is estimated to be 10^{19}–10^{21} Pa·s using the observed geometry and heat flow for accretionary prisms (Emerman and Turcotte, 1983; Furukawa, 1999; Platt, 2000).

At higher temperatures, ductile deformation is dominant, and the creep strength

decreases exponentially with temperature. Laboratory experiments have shown that the viscosity of silicic rocks is 10^{22}–10^{24} Pa·s at 200–400°C for the dislocation creep regime (Gleason and Tullis, 1995; Luan and Paterson, 1992). The viscosity values appear to be several orders of magnitude larger than those estimated from crustal deformation in nature and may provide estimations of the maximum shear strength (Gleason and Tullis, 1995). Other possible softening mechanisms include pressure solution, recrystallization, and reaction softening, which likely reduce the viscosity to values substantially less than those obtained in laboratories (Ranalli and Murphy, 1987).

In accretionary prisms, water is supplied by compaction and dehydration of the accreted sediment and the descending plate (Moore and Vrolijk, 1992); high (lithostatic) pore pressure is expected for propagating fluid conduits formed in the compacting sediment (Brown et al., 1994). Deeper in the accretionary prisms, it is considered that water is continuously released by metamorphic reactions in the descending oceanic crust and sediments (Etheridge et al., 1983; Hacker et al., 2003; Iwamori, 2007) and migrates upward into the overlying crust through a network of microcracks and the megathrust interface (Etheridge et al., 1984; Furukawa, 2009; Saffer, 2007). In water-saturated conditions, solution mass transfer likely becomes dominant under crustal conditions; for paleo-accretionary prisms, the fluid-assisted mass transfer process is the dominant mechanism for viscous deformation in low-temperature and high-pressure metamorphic terranes (Feehan and Brandon, 1999; Moore et al., 2007; Norris and Bishop, 1990; Schwarz and Stöckhert, 1996).

Pressure solution microstructures are commonly observed in rocks which have suffered diagenetic or low metamorphic grade conditions (McClay, 1977), and it is suggested that

pressure solution is not a strongly temperature dependent process (Rutter, 1976). Pressure solution is a mechanism whereby the concentration of normal stress at grain contacts causes local dissolution of the material, transport of the solutes out of the contact site and precipitation of the material on the less stressed faces of the grains (Rutter, 1983). The rate of rock deformation by pressure solution is controlled by the slowest of the three above-mentioned elementary stages. Estimated pressure solution deformation rates may vary by many orders of magnitude (den Brok, 1998) because the fundamental processes are not yet clearly understood (Gratier et al., 2009). The temperature above which the pressure solution becomes the dominant mechanism was estimated to be about 200°C under water-rich conditions in paleo-accretionary complexes (DiTullio and Byrne, 1990; DiTullio et al., 1993; Duebendorfer et al., 1998; Fisher and Byrne, 1992). The deformation rate caused by the pressure solution creep is suggested to have a linear stress dependence, and the viscosity is estimated to be 10^{16}–10^{19} Pa·s at 250–350°C (Shimizu, 1995). In this study, a simple viscosity profile that takes the pressure solution mechanism into account is used; below the transitional temperature (T_{tr}), the viscosity is considered to be constant in the brittle regime described by viscous flow models (Emerman and Turcotte, 1983; Furukawa, 1999; Platt, 2000), and decreases exponentially in the ductile regime above T_{tr}. The viscosity value η (Pa·s) is calculated using the equation as follows,

$$\begin{cases} \eta = \eta_0 & (T < T_{tr}) \\ \eta = a \cdot e^{\frac{b}{T+273}} & (T \geq T_{tr}) \end{cases}$$

where η_0, a, and b are constant. In this study, T_{tr}, η_0, a, and b are set to be 200°C, $5.0 \cdot 10^{20}$ Pa·s, $9.3 \cdot 10^{14}$ Pa·s, and $6.2 \cdot 10^{3}$ K, respectively; the viscosity value at 300°C is about ten times

smaller than that at T_{tr} (Fig. 4).

In this study, the temperature and flow structures induced by the subducting plate are calculated for hot and cold accretionary prisms, and the effect of the temperature-dependent rheology on these structures is estimated. The temperature structure in the accretionary prism is mainly controlled by the age and subduction velocity of the subducting oceanic plate (Molnar and England, 1990; Peacock and Wang, 1999); the temperature in the accretionary prism is expected to increase when the descending plate is younger in age and/or has a slower subduction velocity. In the calculations, ages of the subducting oceanic plates are considered to be 5 and 50 Ma; the maximum thickness of the accretionary prism and the subduction velocity are set to 20 km and 0.045 m/yr, respectively. At the arc side boundary, the temperature profile is calculated using a surface heat flow of 40 mW/m^2 and the thermal conductivity values are listed in Table 1. The arc side boundary of the accretionary prism is set at the location where the horizontal distance from the trench is 1.3 times longer than that of the thrust intersection with the top of the lower crust to avoid the effect of the temperature given at the arc side boundary. The effective frictional coefficient at the base of the accretionary prism is set to 0.02 (Furukawa, 1999; Wang et al., 1995; Wang and Suyehiro, 1999); shear stress, then, increases linearly with depth at the plate interface.

In this study, the temperature and viscous-flow structures in the accretionary prisms for the Cascadia and Nankai subduction zones are also calculated. In the Cascadia subduction zone, the Crescend/Siletz mafic terrane is expected to have higher strength and acts as a backstop. In this study, the boundary between the accreted sediment and mafic terrane is assumed to be located at the coast; the depth of the subducting plate at the coast is assumed to

be 20 km. In the calculations, the subducting plate with an age of 8 Ma (Hyndman and Wang, 1993) is assumed to subduct at a velocity and angle of 0.04 m/yr (DeMets et al., 1990) and 9° (Parsons et al., 1999; Ramachandran et al., 2006), respectively. A one-dimensional temperature profile for a surface heat flow of 40 mW/m^2 is used for the arc side boundary (Blackwell et al., 1990).

In the Nankai subduction zone, the maximum thickness of the accretionary prism is assumed to be 23 km, and the MTL is considered to be the rigid arc side boundary of the accretionary prism across which there is no flux of accreted sediments. The age of the subducting Philippine Sea plate varies along the Nankai trough; in this study area, paleomagnetic studies have estimated the age to be 21–23 Ma (Okino et al., 1999; Sdrolias et al., 2004); an age of 22 Ma is used in this study. The subduction velocity and angle are set to 0.045 m/yr (Seno et al., 1993) and 9° (Kodaira et al., 2003), respectively. At the arc side boundary, the temperature profile is calculated using a surface heat flow of 50 mW/m^2 (Furukawa et al., 1998).

In the Nankai and Cascadia subduction zones, thick sediments are deposited at the trench, and the temperature at the top of the oceanic plate is higher than that at the ocean bottom. In this study, the geotherm of the oceanic lithosphere is estimated by considering the overlying sediment; the temperature at the surface of the oceanic plate is 230 and 90°C for the Cascadia and Nankai subduction zones, respectively (Oleskevich et al., 1999).

Wang et al. (1995) suggested that the age history of the subducting lithosphere is crucial for the estimation of the thermal regime under the Nankai subduction zone. In their thermal model, the estimated temperature along the plate interface at present for the transient case

considering the age history is only about a few tens of degrees higher than that for the steady state with the fixed age of the subducting lithosphere in the region between the trench and coast; thus the age history is not considered in this study.

Results

Hot and cold accretionary prisms

The temperature and flow structures calculated for the accretionary prisms with the young and old subducting oceanic plates are shown in Fig. 5. The temperature in the accretionary prism is higher for younger subducting oceanic plates; in the deeper part of the accretionary prism, the temperature is above 200°C, and ductile deformation is assumed to occur by pressure solution creep. For the colder accretionary prism, the temperature is below 200°C throughout the prism.

The flow patterns for the two accretionary prisms are quite different from each other. For the cold prism, the flow pattern is analogous to a simple corner flow, as shown in Fig. 5(a); this is because the viscosity is constant in the accretionary prism due to the lower temperature. The flow is induced above the interface between the accretionary prism and descending plate and assuming a homogeneous, isotropic prism; the upward flow is located above the intersection between the top of the lower crust and the descending plate, although the rigid vertical boundary is located far arcward of the upward flow. The flow velocity just above the subducting lithosphere is nearly constant throughout the depth and is approximately 0.003 m/yr, which is one order of magnitude lower than the subduction velocity; this indicates that most of the subduction velocity is consumed by thrust

displacements at the plate interface.

For the hot prism (Fig. 5b), sediment accreted at the trench is underthrusted by the drag of the subducting lithosphere; the lower part of the underthrusting flow continues to the deeper part of the prism, whereas the upper part of the flow goes upward in the middle part of the accretionary prism and has a simple corner flow pattern similar to that of the cold accretionary prism. At the rear of the prism, the lower downward flow on the subducting lithosphere reverses and proceeds trenchward. This circulating flow occurs in the deeper part of the accretionary prism, where the viscosity is lower due to the higher temperature ($>T_{tr}$). The circulating flow is overlain by a lid in the overlying higher viscosity layer. The return flow just below the lid reaches the surface between the corner flow region and the lid.

The flow velocity for the downward flow on the subducting plate as it underthrusts deeper into the accretionary prism varies with the depth; the flow velocity is nearly constant under the corner flow region, where the temperature for the downward flow is below T_{tr}. The flow velocity increases with depth in the deeper accretionary prism, where the temperature is higher than T_{tr}, because of the decrease of viscosity. The flow velocity just above the subducting plate is approximately 0.007 m/yr under the corner flow region and increases to approximately 0.035 m/yr near the bottom of the prism.

Cascadia and Nankai accretionary prisms

The calculated temperature and flow patterns for the Cascadia and eastern Nankai subduction zones are shown in Fig. 6. For both the subduction zones, the corner flow pattern and lid on the trench and arc sides of the accretionary prisms, respectively, can be observed; the flow pattern is similar to that of the hot prism as shown in Fig. 5(b). For the eastern

Nankai subduction zone, the trench side of the lid above the interface between the accretionary prism and the subducting plate is narrower than that in the Cascadia subduction zone. In the Nankai subduction zone, the temperature is lower because the older and colder oceanic plate is subducting, and the region of the circulating flow becomes smaller. The return flow tends to uprise in the thicker brittle accretionary prism, resulting in a narrower lid.

Discussion

Hot and cold accretionary prisms

In the cold accretionary prism, the flow induced by the subducting plate is similar to a corner flow (Fig. 5(a)). In this study, the internal deformation caused by fault displacements with the addition of sediment to the trench side of the accretionary prism is expressed by a simple viscous flow model. The corner flow region is, thus, considered to be the part of the accretionary prism, where imbricate thrusts develop due to accretion of off-scraped sediments under older thrust packets because of the drag of the subducting plate.

The arc side of the accretionary prism above the rigid lower crust is almost stagnant, and the upward flow is located in the area above the intersection between the top of the lower crust and the interplate megathrust (Fig. 5(a)). The rigid lower crust acts as a backstop for the induced flow in the accretionary prism, and the outer ridge is formed above the intersection. The outer ridge becomes a barrier for terrigenous sediments from the arc, and the forearc basin is formed in the arc side of the outer ridge.

The corner flow region in the trench side of the hot accretionary prism (Fig. 5(b)) is considered to be the region of imbricate thrusts formed by drag of the subducting plate,

which is similar to the cold accretionary prism. In the arc side of this region, the accreted sediment migrates upward, and the outer ridge is formed in this region, considering that the flux of the return flow decreases due to underplating in the deeper accretionary prism, as described below. The back-arc basin is formed arcward of the outer ridge. In the corner flow region, the upward flow occurs without a backstop, and this region is located above the underthrusting flow on the subducting plate where a constant viscosity is imposed because the temperature is lower than T_{tr}.

The downward flow on the subducting plate circulates in the deeper part of the prism, where the viscosity is lower; the return flow just below the lid proceeds trenchward. This trenchward flow is may be the cause of arc-normal extension in the overlying lid. In the trench side of the accretionary prism, the imbricate thrusts develop by arc-normal compression that is caused by the drag of the subducting plate. In this accretionary prism, the compressional and extensional stresses in the arc-normal direction coexist in the near-surface layer of the accretionary prism.

The return flow reaches the surface in the region between the corner flow region and lid. In the near-surface low-temperature layer, deformation is considered to be caused by fault displacements, as the imbricate thrust region in the trench side of the accretionary prism (Davis et al., 1983), and the accreted sediment carried by the return flow should be extruded by thrust displacements. When the accretionary prism is growing, mainly due to the underplating of sediments carried by the downward flow in the deeper part of the prism (Kimura and Mukai, 1991), the volume flux of the return flow below the lid becomes smaller than that calculated in this study. Then, most of the volume of the return flow might extrude

by thrust movements near the lid rather than broadly over this region, considering the minimization of work necessary to drive the flow. In the region between the extrusion of the return flow and the imbricate thrust region, the upward flow rate may become lower and some deformation may occur. Schematic diagrams of the hot and cold accretionary prisms are shown in Fig. 7.

In this study, a simple model was used to estimate viscous flow and temperature structures in the accretionary prisms. The temperature dependency of viscosity of the accreted sediments used in the calculations has much uncertainty, but the coexistence of the compressional and extensional regions in the accretionary prisms can be predicted using the T_{tr} of 200°C. As the T_{tr} increases, the circulation flow region and the lid become smaller and shorter, respectively. For the T_{tr} greater than about 300°C, the simple corner flow region prevails in the whole prism and the circulation flow region disappears in the hot prism. When the pressure solution process could be effective below 200°C (Gratier, 1987), on the contrary, the lid grows trenchward in the hot prism. The lid cannot exist stably and is detached from the rigid crust arcward of the accretionary prism for the T_{tr} lower than about 100°C. Rheological properties of rocks at low temperatures should be qualitatively estimated for detailed analysis of the deformation and temperature structures in the accretionary prisms.

In most accretionary prisms, a décollement has been observed above the subducting plate, which is considered to be a zone of high pore fluid pressure; this zone detaches the off-scraped sediment deformed by imbricate thrusts from the undeformed sediment overlying the subducting plate (Park et al., 2010; Shi and Wang, 1988; Tobin and Saffer, 2009). The undeformed sediment below a décollement is expected to subduct with nearly the same

velocity as that of the subducting plate; in shallower depths, the décollement acts as the plate interface (Moore, 1989). Deeper in the accretionary prism, the underthrusting sediment is considered to be underplated to form duplex structures (Moore and Byrne, 1987; Kimura et al., 1996; Kimura and Mukai, 1991) In this study, the décollement is not considered to simplify the calculations, and the plate interface is fixed at the surface of the subducting plate. Assuming that the décollement is the top boundary of the underthrusting flow on the subducting plate for the hot accretionary prism, the underthrusting flow layer probably becomes thinner than the result shown in Fig. 5(b) due to a higher underthrusting velocity.

Cascadia

The calculated temperature and flow structures in this region are shown in Fig. 6a, which are similar to those of the hot accretionary prism shown in Fig. 5(b). The corner flow pattern and return flow under the lid can be seen in the trench and arc sides of the prisms, respectively. The layer of the return flow just below the lid shown in this study may correspond to the highly deformed MBF, and the return flow is probably the cause of the arc-normal extension in the upper slope and shelf in this region. The landward-dipping imbricated listric structure of the normal faults supports the hypothesis that the basal drag of the ductile return flow in the trenchward direction causes the extension in the overlying lid (McNeill et al., 2000).

In this region, the extensional structure is observed to be arcward of the CMT, as shown in Fig. 1. The return flow under the lid may extrude at the surface near the lid by displacements of thrusts, as mentioned previously. The CMT could be the most prominent fault where most of the volume flux of the return flow under the lid is extruded as brittle

thrust blocks. In the region between the extruded thrust blocks and the imbricate thrust region, the outflow rate is low and rollover and drape folds may be formed as shown in the seismic reflection profiles (Booth-Rea et al., 2008).

In the trench side of the lower slope of the accretionary prism in this region, landward-vergent thrusts are dominant. This region is considered to correspond to the corner flow region in the calculated flow pattern, where imbricate thrusts are expected to be formed due to drag of the subducting plate. The landward-vergent imbricate thrust packets are suggested to be formed by weak effective friction at the base of the accretionary prism, which is caused by high pore pressure (Byrne et al., 1993; Seely, 1977), a ductile basal layer (Gutscher et al., 2001), and higher temperatures (Booth-Rea et al., 2008). An arcward dipping décollement in addition to the low basal shear stress (MacKay, 1995) and a strong increase in Pleistocene sedimentation rate (Adam et al., 2004) may be the cause of the landward-vergent thrusts. In the lower slope, the thick sediment layer deposited during the high sedimentation rate in the Pleistocene has been shortened by the displacement of the imbricate thrusts; the surface tilt is still very low, and the outer ridge is not observed in the arc side of the lower slope.

In the Cascadia forearc, the mafic Crescent/Siletz volcanic terrane is absent in the shelf and upper slope where the extensional structure is observed (McNeill et al., 1997; Tréhu et al., 1994). In the calculations, the mafic volcanic terrane is considered to be the backstop due to its higher shear strength, and a ductile return flow cannot be expected in a region where the mafic terrane exists under the shelf and upper slope; this is because the area of the low viscosity region becomes smaller and the circulating flow cannot be induced in the deeper accretionary prism. The extensional structures are thus formed in the shelf and upper slope

where the seaward limit of the mafic terrane is located onshore.

Southwest Japan

The calculated deformation structure in Fig. 6b shows similar features to those of the Cascadia subduction zone; a corner flow and lid overlying the return flow can be observed. The trenchward return flow below the lid is likely to be the cause of the normal faults observed at the upper slope and shelf, and the corner flow region is considered to correspond to the trench side of the accretionary prism where imbricate thrusts are well developed. Compared to Cascadia, the ductile region is smaller due to the lower temperature, and the width of the lid in the trench side of the thrust intersection with the top of the lower crust is narrower. In this area, seaward-dipping normal faults are dominant; these faults do not show a listric geometry (Arai et al., 2006), which may be due to the thicker brittle surface layer.

The return flow below the lid at the rear of the accretionary prism may extrude due to thrust displacements near the lid, considering the reduced volume flux of the return flow due to the underplating in a growing accretionary prism, as mentioned previously. The ETS may be the thrust where most of the flux of the return flow is exposed to the surface, which is similar to the CMT in the Cascadia subduction zone. The upward flow rate becomes lower in the domain between the ETS and imbricate thrust region. In the frontal part of the Nankai accretionary prism, the imbricate thrusts are well developed, and the outer ridge is one of the marked bathymetric features. It is considered that the outer ridge and the forearc basin are located in the arc side of the corner flow and the slower upwelling regions, respectively.

When the accretionary prism is thinner, the viscosity contrast becomes smaller for the same temperature structure as that estimated in this study (Fig. 6b). For a thinner accretionary

prism, the pattern of the flow induced by the drag of the subducting plate tends to be similar to a simple corner flow due to the smaller viscosity variation in the accretionary prism, i.e., like the flow pattern in the cold prism shown in Fig. 5(a). In this calculation, the flow induced by the subducting plate becomes similar to a simple corner flow, when the thickness of the accretionary prism is less than approximately 20 km.

When the flow induced by the subducting plate is similar to that of the cold prism shown in Fig. 5(a), the outer ridge is located above the intersection between the top of the lower crust and the interplate megathrust. In the western Nankai accretionary prism, the location of the outer ridge approximately coincides with the seaward limit of the lower crust (Kodaira et al., 2000; Takahashi et al., 2002) (Fig. 2). The lower crust acts as a backstop (Fig. 5). In the frontal part of the accretionary prism, imbricate thrusts develop, and the outer ridge is formed in the arc side of this region. In the region arcward of the outer ridge, the flow is hardly induced (Fig. 5), and the forearc basin is formed.

Location of locked zones

In subduction zones with relatively high temperatures, the circulating flow occurs at the rear of the accretionary prisms (Fig. 6). The flow velocity just above the subducting plate is higher in the deeper accretionary prism than under the imbricate thrust region, and most of the subduction velocity of the underthrusting plate is consumed by ductile deformation in the deep accretionary prism. A small amount of elastic strain then accumulates in this region, although the frictional stress increases with depth. In the calculations, the velocity of the downward flow on the subducting plate in the circulating prism is approximately 60–80% of the subduction velocity. The locked zone of the interplate megathrust is, then, expected to be

located under the area trenchward of the extensional region above the circulating flow. The CMT and ETS are then located approximately above the downdip limit of the locked zones in the Cascadia and eastern part of the Nankai accretionary prisms, respectively.

The updip limit of the interplate thrust has been suggested to be controlled by the illite-smectite transition which occurs at 100–150°C (Hyndman and Wang, 1993). However, recent laboratory experiments have shown that illite does not show unstable frictional behavior (Saffer and Marone, 2003), and other factors including stress, hydration, and quartz content could be important for the stable-unstable sliding transition (Ikari et al., 2007; Moore and Saffer, 2001). In this study, the updip limit is assumed to be controlled by not only the smectite-illite transition but other factors including the rigidity of the compacting sediments, low-grade metamorphic reactions, and pore fluid pressure (Beeler, 2007; Brown et al., 2003; Moore and Saffer, 2001).

In the active dewatering region in the frontal part of the accretionary prism (Saffer and Bekins, 1998), pore pressure is expected to be high. In this region, the compacting sediments may facilitate thrust formation and displacements under high pore pressure conditions (Brown et al., 1994), resulting in the imbricate thrust packet structure. In the Nankai accretionary prism, very low frequency earthquakes are observed in the imbricate thrust region (Ito and Obara, 2006). Together with high content of clay minerals with low frictional coefficients (Brown et al., 2003; Moore and Saffer, 2001), high pore fluid pressure, and low rigidity due to high porosity in the compacting sediments may cause such low frequency events (Beeler, 2007; Dragert et al., 2001; Furukawa, 2009; Obara, 2002; Scholz, 2002). Stable frictional behavior can be expected at the interplate megathrusts in the imbricate thrust

region.

In the region arcward of the outer ridge, the pore fluid pressure is expected to be lower (Bekins and Dreiss, 1992; Saffer and Bekins, 1998). The low pore fluid pressure together with the high rigidity and frictional coefficient due to consolidation caused by low-grade metamorphic processes can result in the stick-slip behavior at the interplate megathrust (Beeler, 2007; Brown et al., 2003; Moore and Saffer, 2001). Then, the updip limit of the locked zone is expected to be located under the arcside of the imbricate thrust region, where the outer ridge can be formed.

In the eastern Nankai subduction zone off the Tokai area, the locked zone at the interplate megathrust is inferred to be located between the extensional zone and the outer ridge; here, the fault slip is unstable and a larger elastic strain can accumulate in the overlying crust. Using GPS data, the back-slip distribution at the megathrust in this region was estimated to be 20–40 mm/yr off the Tokai area (Sagiya, 1999); the higher back-slip (>35 mm/yr) area approximately corresponds to the region between the ETS and outer ridge, as shown in Fig. 2.

In the eastern Nankai subduction zone, the calculated temperature is lower than that in the Cascadia subduction zone (Fig. 6), and the deeper part of the megathrust in contact with the lower crust could be seismic because the lower crust material has a higher shear strength than that in the accretionary prism (Kirby, 1983; Ranalli and Murphy, 1987). Assuming that the downdip limit of the seismogenic zone at the megathrust coincides with the 350°C isotherm (Hyndman et al., 1995), the deeper seismic zone at the megathrust is at a depth of 23–26 km, as shown in Fig. 6b. A locked zone at the megathrust was estimated using

microseismicity data at the megathrust in the depth of 20–30 km under the Tokai area (Matsumura, 1997); this depth of the locked zone agrees with the depth of the deeper locked zone estimated in this study.

In the western and central Nankai accretionary prisms, the locked zone is expected to be located arcward of the outer ridge. In Fig. 2, the coseismic slip distribution for the earthquakes in 1944 and 1946 in the Nankai subduction megathrust estimated using geodetic data is also shown (Sagiya and Thatcher, 1999). The trenchward limit of the larger coseismic slip area agrees with the outer ridge, and the transition of the stable-unstable frictional regime at the interplate megathrust may be located below the outer ridge. The slip off the Kii peninsula is smaller than that off the Shikoku Island. The overlying crust on the locked zone off the Kii peninsula may be composed of consolidating sediments; the fluid-assisted ductile deformation mechanisms may work inefficiently and release part of the elastic strain accumulating in this zone. The downdip limit may be located at the ~350°C isotherm or the Moho interface (Hyndman et al., 1995).

In the frontal part of the Cascadia accretionary prism, landward-vergent imbricate thrusts are dominant, which is suggested to be caused by high pore fluid pressure resulting from high sedimentation rate in the Pleistocene (Byrne et al., 1993; Seely, 1977). In this region, slip at the interplate megathrust may be stable and aseismic, as that suggested in the Nankai subduction zone in this study.

Reflection seismic profiles show that the zone between the imbricate thrust region and CMT is characterized mostly by folds without thrusts (Booth-Rea et al., 2008). In the upper slope region arcward of the CMT, most of the downdip displacement of the subducting plate

is consumed by ductile deformation in the overlying accretionary prism. A small amount of elastic strain may accumulate in this ductile part of the accretionary prism, as in the eastern Nankai subduction zone. A locked zone may develop under the fold zone between the imbricate thrust region and CMT, as shown in Figs. 1 and 6a.

The low gravity in the forearc is supposed to be a proxy for the locked zones of the long-term coseismic slip at the interplate megathrust; in the Cascadia subduction zone, locked zones are suggested to be located under the upper slope and shelf (Wells et al., 2003). In this study, the deeper accretionary prism under the upper slope and shelf where the extensional structure is observed is inferred to be in the ductile regime. The elastic strain that accumulated at the rear of the accretionary prism under the extensional region is probably small, and large coseismic slip could not be expected in this region. In the northern and southern segments of the Cascadia subduction zones, the mafic volcanic terrane is located onshore; the contact between the mafic terrane and subducting plate could be in the unstable slip regime, and the locked zone may be located under the upper slope and shelf.

The interplate frictional coupling was modeled using geodetic data from the Cascadia subduction zone. In the models, the locked zone at the plate interface was assumed to be from the deformation front to the 350°C isotherm at the plate interface as estimated from thermal models (Flück et al., 1997). Other models that consider deeper locked zones can also explain the observed surface displacements (Stanley and Villasenor, 2000). The interplate frictional coupling could not be well constrained according to current geodetic data for the Cascadia subduction zone.

In hot prisms such as the Cascade and eastern Nankai, the location of the locked zone is

controlled by the ductile flow in the prism and is located between the imbricate thrust region and the extensional zone; the outer ridge is formed at the arc side of the thrust region. For cold prisms, the up-dip limit of the locked zone is located under the outer ridge at the arc side of the thrust region where the top of the lower crust contacts with the subducting plate; the lower crust acts as a backstop. In both cases, the fore-arc basin can be formed above the locked zone. Such spatial relation between the locked zone and the forearc basin was shown in some subduction zones (Wells et al., 2003). Schematic figures of the hot and cold prisms are shown in Fig. 7.

It is suggested that distribution of locked zones at the interplate megathrust is controlled by the spatial variation of fluid pressure in the subducting plate and overlying crust at the Hikurangi subduction zone (Fagereng and Ellis, 2009; Reyners and Eberhart-Phillips, 2009); temperature at the plate interface with lower fluid pressure could become higher due to higher interplate frictional stress, which causes the interplate zone to be ductile and aseismic (Fagereng and Ellis, 2009). The variation of the frictional stress may control the interplate coupling strength, but the frictional stress of up to 200 MPa is required to control the rheology of the megathrust zone (Fagereng and Ellis, 2009). This stress value is much higher than those estimated in the other subduction zones (Furukawa, 1999; Wang et al., 1995; Wang and Suyehiro, 1999). In this study, the spatial relation between the locked zone and the surface features including the stress state, the forearc basin, and the imbricate thrusts in the subduction zones can be explained using the relatively low frictional stress estimated previously.

Conclusions

Deformation in accretionary prisms is calculated using a simple viscous model that considers the temperature-dependent viscosity. The results reveal that accreted sediment that is underthrusted to large depths in the accretionary prisms circulates under a lid at the rear of the hot prisms. Most of the prism material in the return flow may extrude by thrust displacements near the lid, considering the decrease of the flux of the return flow due to underplating in the growing accretionary prism (Kimura and Mukai, 1991). A simple corner flow pattern is calculated for the frontal part of the hot accretionary prisms. In this region, off-scraped sediment accretes at the bottom of the overlying crust, and the imbricate thrust packets develop due to the drag of the subducting plate; the trajectory of accreted sediment becomes similar to that of a simple corner flow. In cold prisms, the return flow is not developed, and the simple corner flow pattern is dominant throughout the prism. An outer ridge is formed at the arc side of the corner flow region, where the upheaval velocity is larger due to underthrusting of the thrust packets; the forearc basin can then be formed arcward of the outer ridge.

In the eastern Nankai subduction zone and the Cascadia subduction zone off Washington and the northern Oregon, the arc-normal extensional stress in the imbricate thrust region at the rear of the accretionary prisms coexists with the arc-normal compressional stress in the normal fault region at the front in these subduction zones. The calculated temperature and flow pattern for the Cascadia and eastern Nankai subduction zones are like those for the hot prism, and this stress state is probably caused by the return flow under the lid in the hot accretionary prism with variation of viscosity.

In the corner flow region with well developed imbricate thrusts, the interplate megathrust under the region may be aseismic (Beeler, 2007; Byrne et al., 1988) due to the high pore fluid pressure (Bekins and Dreiss, 1992; Saffer and Bekins, 1998) and the high concentration of clay minerals (Ikari et al., 2007; Moore and Lockner, 2004). In the region arcward of the outer ridge, the accreted sediment is likely to be consolidated enough under low-grade metamorphic conditions to cause an unstable seismic slip at the interplate megathrust (Beeler, 2007; Byrne et al., 1988; Moore and Saffer, 2001). At the rear of the accretionary prisms under the extensional zone where the accreted material circulates under the lid, the model results in this study show that more than 60–80% of the subduction velocity is consumed by the ductile deformation, and a small amount of elastic strain could be accumulated in this region. Larger elastic strain is thus accumulated between the imbricate thrust and extensional regions in the hot accretionary prism including those at the Nankai and Cascadia subduction zones; a larger coseismic slip is expected in this region. In cold prisms, locked zones are expected to be located arcward of the outer ridge. Locked zones at the interplate megathrust are thus located under the forearc basin in subduction zones where the forearc basin is developed.

In the eastern Nankai subduction zone off the Tokai area, the estimated temperature is lower than that in Cascadia and the lower crust may be in the unstable slip regime. Another locked zone is thus expected at the depth of the lower crust. The depth range of the locked zone is estimated to be 23–26 km in this study, assuming that the downdip limit of the seismogenic zone at the megathrust coincides with the 350°C isotherm (Hyndman et al., 1995).

The location of the outer ridge in the western and central Nankai subduction zones is considered to be controlled by the location of the trenchward limit of the lower crust and the splay-fault, respectively. Locked zone is thus located under the forearc basins arcward of the outer ridge.

In the Cascadia subduction zone, a part of the interplate megathrust under the imbricate thrust region is expected to be aseismic as is the case in the Nankai subduction zone, whereas the elastic strain is mostly consumed by ductile deformation in the deeper accretionary prism under the extensional structures. A larger coseismic slip is thus expected in the zone between the imbricate thrust region on the lower slope and the Cascadia main thrust which is the trenchward limit of the extensional zone.

Acknowledgements

I am grateful to the reviewers for their constructive and useful comments. I would like to thank Kyoto university library for providing us convenient work spaces. I also thank T. Ohata for supporting and encouraging me to revise the manuscript.

References

Adam, J., Klaeschen, D., Kukowski, N. and Flueh, E., 2004. Upward delamination of Cascadia Basin sediment infill with landward frontal accretion thrusting caused by rapid glacial age material flux. Tectonics, 23: TC3009.

Arai, K. et al., 2006. Active faults and tectonics on the upper forearc slope off Hamamatsu city, central Japan. J. Geol. Soc. Japan, 112: 749-759 (in Japanese with English abstract).

Beeler, N.M., 2007. Laboratory-observed faulting in intrinsically and apparently weak materials. In: T.H. Dixon and J.C. Moore (Editors), The Seismogenic Zone of Subduction Thrusts Faults. Columbia Univ. Press, New York, pp. 370-449.

Bekins, B.A. and Dreiss, S.J., 1992. A simplified analysis of parameters controlling dewatering in accretionary prisms. Earth Planet. Sci. Lett., 109: 275-287.

Blackwell, D.D., Steele, J.L. and Kelley, S., 1990. Heat flow in the state of Washington and thermal conditions in the Cascade range. J. Geophys. Res., 95: 19495-19516.

Booth-Rea, G., Klaeschen, D., Grevemeyer, I. and Reston, T., 2008. Heterogeneous deformation in the Cascadia convergent margin and its relation to thermal gradient (Washington, NW USA). Tectonics, 27: TC4005.

Brown, K.M., Bekins, B.A., Clennell, B., Dewhurst, D. and Westbrook, G., 1994. Heterogeneous hydrofracture development and accretionary fault dynamics. Geology, 22: 259-262.

Brown, K.M., Kopf, A., Undrewood, M.B. and Weinberger, J.L., 2003. Compositional and fluid pressure controls on the state of stress on the Nankai subduction thrust: A weak

plate boundary. Earth Planet. Sci. Lett., 214: 589-603.

Byrne, D.E., Davis, D.M. and Sykes, L.R., 1988. Loci and maximum size of thrust earthquakes and the mechanics of the shallow region of subduction zones. Tectonics, 7: 833-857.

Byrne, D.E., Wang, W. and Davis, D.M., 1993. Mechanical role of backstops in the growth of forearcs. Tectonics, 12: 123-144.

Cowan, D.S. and Silling, R.M., 1978. A dynamic, scaled model of accretion at trenches and its implications for the tectonic evolution of subduction complexes. J. Geophys. Res., 83: 5389-5396.

Dahlen, F.A. and Barr, T.D., 1989. Brittle frictional mountain building 1. Deformation and mechanical energy budget. J. Geophys. Res., 94: 3906-3922.

Davis, D., Suppe, J. and Dahlen, F.A., 1983. Mechanics of fold-and thrust belts and accretionary wedges. J. Geophys. Res., 88: 1153-1172.

DeMets, C., Gorndon, R.G., Argus, D.F. and Stein, S., 1990. Current plate motions. Geophys. J. Int., 101: 425-478.

den Brok, S.W.J., 1998. Effect of microcracking on pressure-solution strain rate: the Gratz grain boundary model. Geology, 26: 915-918.

DiTullio, L. and Byrne, T., 1990. Deformation paths in the shallow levels of an accretionary prism: The Eocene Shimanto belt of southwest Japan. Geol. Soc. Am. Bull., 102: 1420-1438.

DiTullio, L., Laughland, M.M. and Byrne, T., 1993. Thermal maturity and constraints on deformation from illite crystallinity and vitrinite reflectance in the shallow levels of

an accretionary prism: Eocene-Oligocene Shimanto Belt, southwest Japan. In: M.B. Underwood (Editor), Thermal Evolution of the Tertiary Shimanto Belt, Southwest Japan: An Example of Ridge-Trench Interaction. Special Paper. Geol. Soc. Am., Boulder, pp. 63-82.

Dragert, H., Wang, K. and James, T.S., 2001. A silent slip event on the deeper Cascadia subduction interface. Science, 292: 1525-1528.

Duebendorfer, E.M., Vermilye, J., Geiser, P.A. and Davis, T.L., 1998. Evidence for aseismic deformation in the western Transverse Ranges, southern California: Implications for seismic risk assessment. Geology, 26: 271-274.

Emerman, S.H. and Turcotte, D.L., 1983. A fluid model for the shape of accretionary wedges. Earth Planet. Sci. Lett., 63: 379-384.

Etheridge, M.A., Wall, V.J., Cox, S.F. and Vernon, R.H., 1984. High pore pressure during regional metamorphism and deformation: implications for mass transport and deformation mechanisms. J. Geophys. Res., 89: 4344-4358.

Etheridge, M.A., Wall, V.J. and Vernon, R.H., 1983. The role of the fluid phase during regional metamorphism and deformation. J. Metamor. Geol., 1: 205-226.

Fagereng, A. and Ellis, S., 2009. On factors controlling the depth of interseismic coupling on the Hikurangi subduction interface, New Zealand. Earth Planet. Sci. Lett., 278: 120-130.

Feehan, J.G. and Brandon, M.T., 1999. Contribution of ductile flow to exhumation of low-temperature, high-pressure metamorphic rocks: San Juan-Cascade nappes, NW Washington State. J. Geophys. Res., 104: 10883-10902.

Fisher, D.M. and Byrne, T., 1992. Strain variation in an ancient accretionary complex: Implications for forearc evolution. Tectonics, 11: 330-347.

Flück, P., Hyndman, R.D. and Wang, K., 1997. Three-dimensional dislocation model for great earthquakes of the Cascadia subduction zone. J. Geophys. Res., 102: 20539-20550.

Furukawa, Y., 1993. Depth of the decoupling plate interface and thermal structure under arcs. J. Geophys. Res., 98: 20005-20014.

Furukawa, Y., 1995. Temperature structure in the crust of the Japan arc and the thermal effect of subduction. In: M.L. Gupta and M. Yamano (Editors), Terrestrial Heat Flow and Geothermal Energy in Asia. Oxford and IBH Publishers, New Dehli, pp. 203-219.

Furukawa, Y., 1999. Interplate coupling and deformation in the accretionary prism in the Southwest Japan subduction zone. Geophys. Res. Lett., 26: 3145-3148.

Furukawa, Y., 2009. Convergence of aqueous fluid at the corner of the mantle wedge: Implications for a generation mechanism of deep low-frequency earthquakes. Tectonophys., 469: 85-92.

Furukawa, Y., Shinjoe, H. and Nishimura, S., 1998. Heat flow in the southwest Japan arc and its implication for thermal processes under arcs. Geophys. Res. Lett., 25: 1087-1090.

Gleason, G.C. and Tullis, J., 1995. A flow law for dislocation creep of quartz aggregates determined with the molten salt cell. Tectonophys., 247: 1-23.

Gratier, J.P., 1987. Pressure solution-deposition creep and associated tectonic differentiation in sedimentary rocks. In: M.E. Jones and R.M.F. Preston (Editors), Deformation of Sediments and Sedimentary Rocks. Special Publications. Geol. Soc. London, London,

pp. 25-38.

Gratier, J.P., Guiguet, R., Renard, F., Jenatton, L. and Bernard, D., 2009. A pressure solution creep law for quartz from indentation experiments. J. Geophys. Res., 114: B03403.

Gutscher, M.A., Klaeschen, D., Flueh, E. and Malavieille, J., 2001. Non-Coulomb wedge, wrong-way thrusting, and natural hazards in Cascadia. Geology, 29: 379-382.

Hacker, B.R., Peacock, S.M., Abers, G.A. and Holloway, S.D., 2003. Subduction factory 2. Are intermediate-depth earthquakes in subducting slabs linked to metamorphic dehydration reactions? J. Geophys. Res., 108: 11.

Hirose, I. and Ito, K., 2007. P-wave velocity structure beneath the Kinki district from seismic explosion experiments. Ann. Disas. Prev. Res. Inst. Kyoto Univ., 50: 333-341 (In Japanese with English abstract).

Hyndman, R.D. and Wang, K., 1993. Thermal constraints on the zone of major thrust earthquake failure: the Cascadia subduction zone. J. Geophys. Res., 98: 2039-2060.

Hyndman, R.D., Wang, K. and Yamano, M., 1995. Thermal constraints on the seismogenic portion of the southwestern Japan subduction thrust. J. Geophys. Res., 100: 15373-15392.

Ikari, M.J., Saffer, D.M. and Marone, C., 2007. Effect of hydration state on the frictional properties of montmorillonite-based fault gauge. J. Geophys. Res., 112: B06423.

Ito, Y. and Obara, K., 2006. Dynamic deformation of the accretionary prism excites very low frequency earthquakes. Geophys. Res. Lett., 33: L02311.

Iwamori, H., 2007. Transportation of H_2O beneath the Japan arcs and its implications for global water circulation. Chem. Geol., 239: 182–198.

Karig, D.E. and Sharman III, G.F., 1975. Subduction and accretion in trenches. Geol. Soc. Am. Bull., 86: 377-389.

Kimura, G., Maruyama, S., Isozaki, Y. and Terabayashi, M., 1996. Well-preserved underplating structure of the jadeitized Franciscan complex, Pacheco Pass, California. Geology, 24: 75-78.

Kimura, G. and Mukai, A., 1991. Underplated units in as accretionary complex: Melange of the Shimanto Belt of Eastern Shikoku, Southwest Japan. Tectonics, 10: 31-50.

Kirby, S., 1983. Rheology of the lithosphere. Rev. Geophys. Space Phys., 21: 1458-1487.

Kodaira, S. et al., 2003. Cyclic ridge subduction at an inter-plate locked zone off central Japan. Geophys. Res. Lett., 30: 72.

Kodaira, S. et al., 2000. Western Nankai trough seismogenic zone: results from a wide-angle ocean bottom seismic survey. J. Geophys. Res., 105: 5887-5905.

Lachenbruch, A.H., 1970. Crustal temperature and heat production: implications of the linear heat-flow relation. J. Geophys. Res., 75: 3291–3300.

Liu, J. and Ranalli, G., 1998. Stresses and velocities in orogenic wedges with power-law rheology and linearly varying longitudinal strain rate. J. Struct. Geol., 20: 1611-1623.

Luan, F.C. and Paterson, M.S., 1992. Preparation and deformation of synthetic aggregates of quartz. J. Geophys. Res., 97: 301-320.

MacKay, M.E., 1995. Structural variation and landward vergence at the toe of the Oregon accretionary prism. Tectonics, 14: 1309-1320.

Matsumura, S., 1997. Focal zone of a future Tokai earthquake inferred from the seismicity pattern around the plate interface. Tectonophys., 273: 271-291.

McClay, K.R., 1977. Pressure solution and Coble creep in rocks. J. Geol. Soc. London, 134: 71-75.

McNeill, L.C., Goldfinger, C., Kulm, L.D. and Yeats, R.S., 2000. Tectonics of the Neogene Cascadia forearc basin: Investigations of a deformed late Miocene unconformity. Geol. Soc. Am. Bull., 112: 1209-1224.

McNeill, L.C., Piper, K.A., Goldfinger, C., Kulm, L.D. and Yeats, R.S., 1997. Listric normal faulting on the Cascadia continental margin. J. Geophys. Res., 102: 12123-12138.

Molnar, P. and England, P., 1990. Temperatures, heat flux, and frictional stress near major thrust faults. J. Geophys. Res., 95: 4833-4856.

Moore, J.C. and Byrne, T., 1987. Thickening of fault zones: A mechanism of melange formation in accreting sediments. Geology, 15: 1040-1043.

Moore, D.E. and Lockner, D.A., 2004. Crystallographic controls on the frictional behavior of dry and water-saturated sheet structure minerals. J. Geophys. Res., 109: B03401.

Moore, G.F. et al., 2007. Three-dimensional splay fault geometry and implications for tsunami generation. Science, 318: 1128-1131.

Moore, J.C., 1989. Tectonics and hydrogeology of accretionary prisms: role of the décollement zone. J. Struct. Geol., 11: 95-106.

Moore, J.C., Rowe, C. and Meneghini, F., 2007. How accretionary prisms elucidate seismogenesis in subduction zones. In: T.H. Dixon and J.C. Moore (Editors), The Seismogenic Zone of Subduction Thrusts Faults. Columbia Univ. Press, New York, pp. 288-315.

Moore, J.C. and Saffer, D., 2001. Updip limit of the seismogenic zone beneath the

accretionary prism of southwest Japan: An effect of diagenetic to low-grade metamorphic processes and increasing effective stress. Geology, 29: 183-186.

Moore, J.C. and Vrolijk, P., 1992. Fluids in accretionary prisms. Rev. Geophys., 30: 113-135.

Nakanishi, A. et al., 2008. Detailed structural image around splay-fault branching in the Nankai subduction seismogenic zone: results from a high-density ocean bottom seismic survey. J. Geophys. Res., 113: B03105.

Nakanishi, A. et al., 1998. Detailed subduction structure across the eastern Nankai Trough obtained from ocean bottom seismographic profiles. J. Geophys. Res., 103: 27151-27168.

Nakanishi, A. et al., 2002. Crustal structure across the coseismic rupture zone of the 1944 Tonankai earthquakes, the central Nankai Trough seismogenic zone. J. Geophys. Res., 107: EPM2.

Norris, R.J. and Bishop, D.G., 1990. Deformed conglomerates and textural zones in the Otago Schists, South Island, New Zealand. Tectonophys., 174: 331-349.

Obara, K., 2002. Nonvolcanic deep tremor associated with subduction in Southwest Japan. Science, 296: 1679-1681.

Okino, K., Ohara, Y., Kasuga, S. and Kato, Y., 1999. The Philippine Sea: new survey results reveal the structure and the history of the marginal basins. Geophys. Res. Lett., 26: 2287-2290.

Oleskevich, D.A., Hyndman, R.D. and Wang, K., 1999. The updip and downdip limits to great subduction earthquakes: Thermal and structural models of Cascadia, south Alaska, SW Japan, and Chile. J. Geophys. Res., 104: 14965-14991.

Park, J., Tsuru, T., Kodaira, S., Cummins, P.R. and Kaneda, Y., 2002. Splay fault branching along the Nankai subduction zone. Science, 297: 1157-1160.

Park, J. et al., 2010. A low-velocity zone with weak reflectivity along the Nankai subduction zone. Geology, 38: 283-286.

Parsons, B. and Sclater, J.G., 1977. An analysis of the variation of ocean floor bathymetry and heat flow with age. J. Geophys. Res., 82: 803-827.

Parsons, T., Wells, R.E., Fisher, M.A., Flueh, E. and Brink, U.S., 1999. Three-dimensional velocity structure of Siletzia and other accreted terranes in the Cascadia forearc of Washington. J. Geophys. Res., 104: 18015-18039.

Peacock, S.M. and Wang, K., 1999. Seismic consequences of warm versus cool subduction metamorphism: examples from Southwest and Northeast Japan. Science, 286: 937-939.

Platt, J.P., 1986. Dynamics of orogenic wedges and the uplift of high-pressure metamorphic rocks. Geol. Soc. Am. Bull., 97: 1037-1053.

Platt, J.P., 2000. Calibrating the bulk rheology of active obliquely convergent thrust belts and forearc wedges from surface profiles and velocity distributions. Tectonics, 19: 529-548.

Ramachandran, K., Hyndman, R.D. and Brocher, T.M., 2006. Regional P wave velocity structure of the northern Cascadia subduction zone. J. Geophys. Res., 111: B12301.

Ranalli, G. and Murphy, D.C., 1987. Rheological stratification of the lithosphere. Tectonophys., 132: 281-295.

Reyners, M. and Eberhart-Phillips, D., 2009. Small earthquakes provide insight into plate

coupling and fluid distribution in the Hikurangi subduction zone, New Zealand. Earth Planet. Sci. Lett., 282: 299-305.

Rutter, E.H., 1976. The kinetics of rock deformation by pressure solution. Phil. Trans. R. Soc. London, A283: 203-219.

Rutter, E.H., 1983. Pressure solution in nature, theory and experiment. J. Geol. Soc. London, 140: 725-740.

Saffer, D.M. and Bekins, B.A., 1998. Episodic fluid flow in the Nankai accretionary complex: Timescale, geochemistry, flow rates, and fluid budget. J. Geophys. Res., 103: 30351-30370.

Saffer, D.M. and Marone, C., 2003. Comparison of smectite- and illite-rich gouge frictional properties: application to the updip limit of the seismogenic zone along subduction megathrusts. Earth Planet. Sci. Lett., 215: 219-235.

Saffer, D., 2007. Pore pressure within underthrust sediment in subduction zones. In: T.H. Dixon and J.C. Moore (Editors), The Seismogenic Zone of Subduction Thrusts Faults. Columbia Univ. Press, New York, pp. 171-209.

Sagiya, T., 1999. Interplate coupling in the Tokai District, Central Japan, deduced from continuous GPS data. Geophys. Res. Lett., 26: 2315-2318.

Sagiya, T. and Thatcher, W., 1999. Coseismic slip resolution along a plate boundary megathrust: The Nankai Trough, southwest Japan. J. Geophys. Res., 104: 1111-1129.

Scholz, C.H., 2002. The Mechanics of Earthquakes and Faulting. Cambridge Univ. Press, New York, 496 pp.

Schwarz, S. and Stöckhert, B., 1996. Pressure solution in siliciclastic HP-LT metamorphic

rocks - constraints on the state of stress in deep levels of accretionary complexes. Tectonophys., 255: 203-209.

Sdrolias, M., Roest, W.R. and Müller, R.D., 2004. An expression of Philippine Sea plate rotation: the Parece Vela and Shikoku basins. Tectonophys., 394: 69-86.

Seely, D.R., 1977. The significance of landward vergence and oblique structural trends on trench inner slopes. In: M. Talwani and W.C. Pitman (Editors), Island Arcs, Deep Sea Trenches, and Back-Arc Basins. Maurice Ewing Ser. AGU, Washington, D.C., pp. 187-198.

Seno, T., Stein, S. and Gripp, A.E., 1993. A model for the motion of the Philippine Sea plate consistent with NUVEL-1 and geological data. J. Geophys. Res., 98(B10): 17,941-17,948.

Shi, Y. and Wang, C.-Y., 1988. Generation of high pore pressures in accretionary prisms: Inferences from the Barbados subduction complex. J. Geophys. Res., 93: 8893-8910.

Shimizu, I., 1995. Kinetics of pressure solution creep in quartz: Theoretical considerations. Tectonophys., 245: 121-134.

Stanley, D. and Villasenor, A., 2000. Models of downdip frictional coupling for the Cascadia megathrust. Geophys. Res. Lett., 27: 1551-1554.

Takahashi, N. et al., 2002. Seismic structure of western end of the Nankai trough seismogenic zone. J. Geophys. Res., 107: 2212.

Tobin, H.J. and Saffer, D., 2009. Elevated fluid pressure and extreme mechanical weakness of a plate boundary thrust, Nankai Trough subduction zone. Geology, 37: 679-682.

Tréhu, A.M. et al., 1994. Crustal architecture of the Cascadia forearc. Science, 266: 237-243.

von Huene, R. and Scholl, D.W., 1991. Observations at convergent margins concerning sediment subduction, subduction erosion, and the growth of continental crust. Rev. Geophys., 29: 279-316.

Wang, K., Mulder, T., Rogers, G.C. and Hyndman, R.D., 1995. Case for very low coupling stress on the Cascadia subduction fault. J. Geophys. Res., 100: 12,907-12,918.

Wang, K. and Suyehiro, K., 1999. How does plate coupling affect crustal stresses in Northeast and Southwest Japan? Geophys. Res. Lett., 26: 2307-2310.

Wells, R.E., Blakely, R.J., Sugiyama, Y., Scholl, D.W. and Dinterman, P.A., 2003. Basin-centered asperities in great subduction zone earthquakes: A link between slip, subsidence, and subduction erosion? J. Geophys. Res., 108: ESE16.

Yamaji, A., Sakai, T., Arai, K. and Okamura, Y., 2003. Unstable forearc stress in the eastern Nankai subduction zone for the last 2 million years. Tectonophys., 369: 103-120.

Figure Captions

Fig. 1. Tectonic map of the Cascadia subduction zone. The hatched area and gray dashed line denote the region of the extensional structure (Adam et al., 2004; Booth-Rea et al., 2008) and the seaward border of the continental shelf, respectively. CMT represents the Cascadia main thrust (Booth-Rea et al., 2008). The dense gray area denotes the locked zone at the interplate megathrust estimated in this study. The inset is the schematic cross section from reflection seismic studies along the line shown as the thin gray line; the height of the inset corresponds to 5 km (after Booth-Rea et al., 2008).

Fig. 2. Tectonic map of the Nankai subduction zone in southwest Japan. The hatched area denotes the zone where imbricate normal faults are observed. The forearc basins and seaward border of the shelf are shown as light gray areas and the gray dashed line, respectively. ETS and MTL denote the Ensyu thrust system and the Median Tectonic Line, respectively. The gray lines off the Shikoku Island and Kii peninsula represent the contour of the coseismic slip in meters (Sagiya and Thatcher, 1999). The area with a back-slip of >35 mm/yr estimated from GPS data (Sagiya, 1999) and the locked zone estimated from microseismicity data (Matsumura, 1997) are shown as gray dotted lines off and in the Tokai area, respectively. The thick lines denote the location of the intersection between the megathrust and top of the lower crust (Hirose and Ito, 2007; Nakanishi et al., 1998; Nakanishi et al., 2002; Takahashi et al., 2002). The inset is the schematic cross section from reflection seismic studies along the line shown as the thin gray line; the height of the inset corresponds to the two way travel time of 4 s (after Arai et al., 2006).

Fig. 3. Model geometry used in the calculations. The accretionary prism is deformed by the drag of the subducting plate. θ denotes the subduction angle. The dotted rectangle denotes the region shown in Figs. 5 and 6.

Fig. 4. Viscosity-temperature profile used in this study. T_{tr} denotes the transition temperature between the constant viscosity and temperature-dependent viscosity regimes.

Fig. 5. Calculated streamlines and isotherms for (a) hot and (b) cold accretionary prisms. The contour interval for temperature is 100°C. The contour interval for the streamline in (b) is half of that in (a). iTF, iNF, OR, and FB represent the imbricate thrust faults, imbricate normal faults, outer ridge, and forearc basin, respectively. Thick and dense gray areas represent the imbricate thrust region and the lid, respectively. The gray line denotes the location of locked zones at the interplate megathrust estimated in this study. The numbers denote temperature (°C).

Fig. 6. Calculated streamlines and isotherms for (a) the Cascadia, and (b) eastern Nankai subduction zones. The symbols and contour intervals are the same as those in Fig. 5. The numbers denote temperature (°C).

Fig. 7. Schematic diagram of hot and cold accretionary prisms. The dashed line denotes the décollement. Sediment below the décollement is underthrusted and underplated deeper in the accretionary prism. In growing hot prisms, the flux of the return flow under the lid is smaller than that of the underthrusted sediment below the décollement. The return flow is located above the interface between the slab and upper crust and is extruded by thrust

displacements near the lid. In growing cold prisms, the corner flow region is located trenchward of the lower crust, and the outer ridge is formed above the trenchward limit of the lower crust. The thick gray lines represent the location of the locked zones; the interface between the slab and lower crust is expected to be locked, when the temperature at the interface is low enough to be in the brittle regime. UC and LC denote the upper and lower crusts, respectively.

Table 1. Thermal Parameters

	k (W/m·K)	H (μW/m^3)
upper crust and prism	2.5	1.0
lower crust	2.0	0.4
subducting plate	2.9	0.0

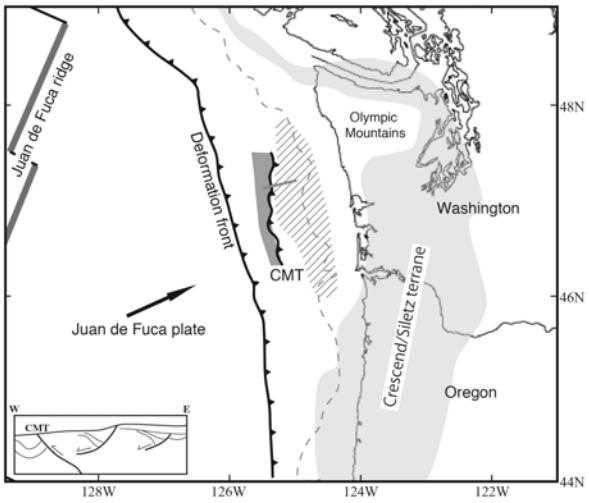
Juan de Fuca ridge
Deformation front
CMT
Juan de Fuca plate
Olympic
Mountains
Washington
Crescend/Siletz terrane
Oregon
W
E
CMT
48N
46N
44N
128W
126W
124W
122W

Fig. 1

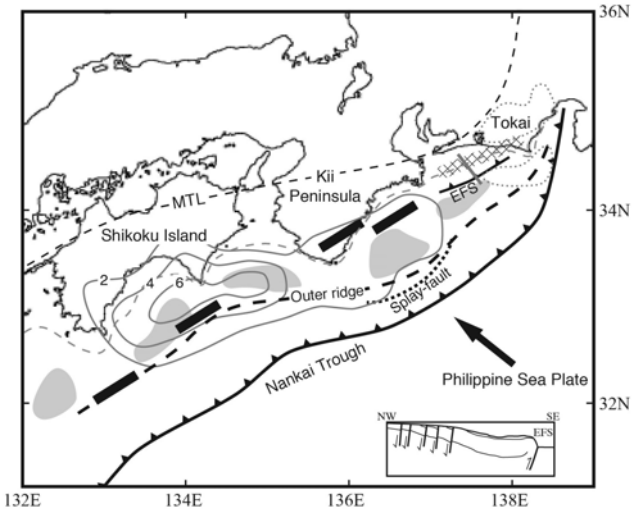
36N
34N
32N
132E
134E
136E
138E
Tokai
Kii
Peninsula
MTL
EFS
Shikoku Island
2
4
6
Outer ridge
Splay fault
Nankai Trough
Philippine Sea Plate
NW
SE
EFS

Fig. 2

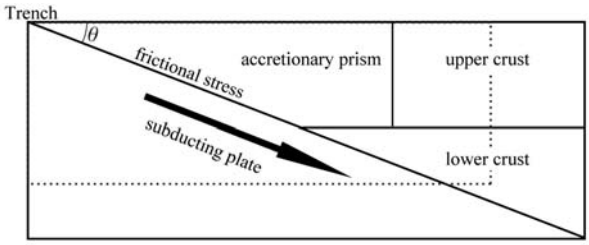
Trench
θ
frictional stress
accretionary prism
upper crust
subducting plate
lower crust

Fig. 3

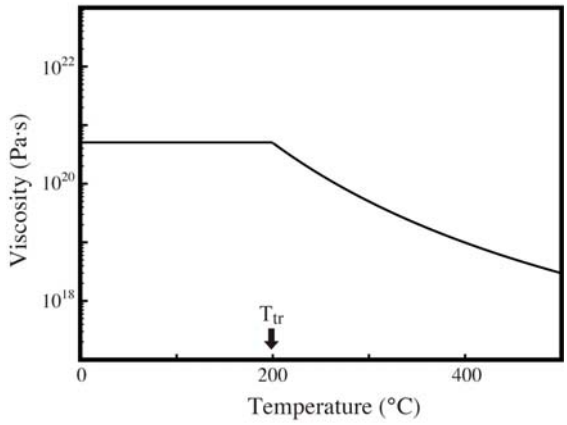

Fig. 4

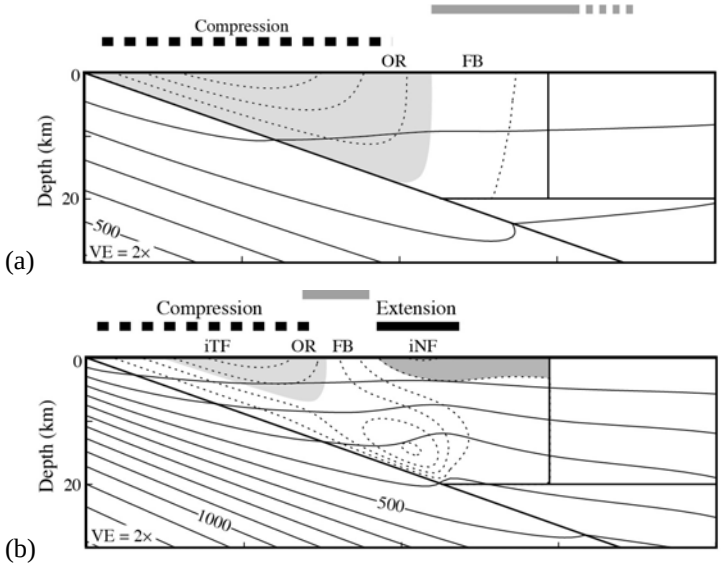
Compression
OR
FB
0
Depth (km)
20
500
VE = 2×
(a)
Compression
Extension
iTF
OR
FB
iNF
0
Depth (km)
20
500
1000
VE = 2×
(b)

Fig. 5

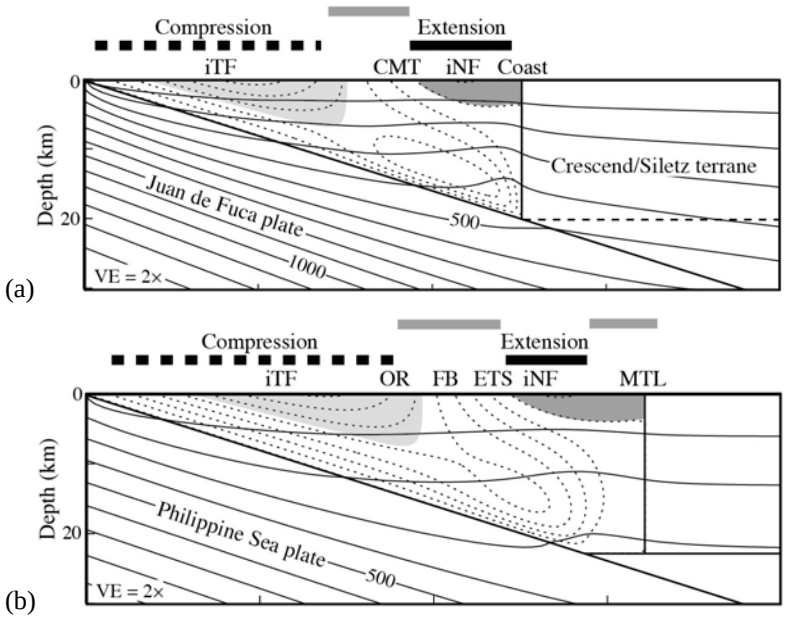
Compression
Extension
iTF
CMT
iNF
Coast
0
Depth (km)
20
Juan de Fuca plate
Crescend/Siletz terrane
500
1000
VE = 2×
(a)
Compression
Extension
iTF
OR
FB
ETS
iNF
MTL
0
Depth (km)
20
Philippine Sea plate
500
VE = 2×
(b)

Fig. 6

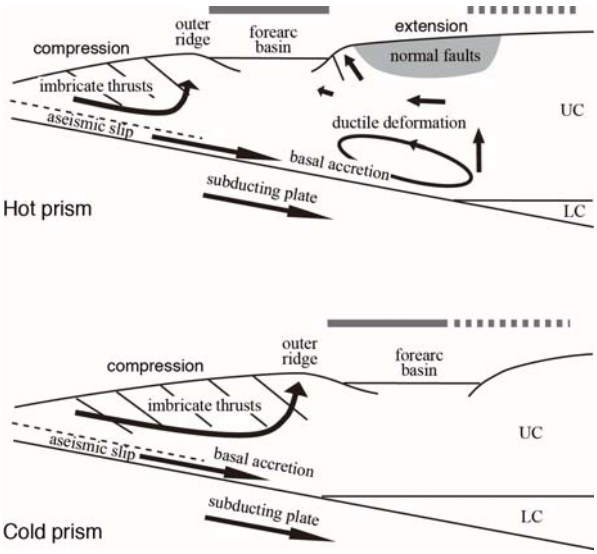
outer ridge
forearc basin
extension
compression
normal faults
imbricate thrusts
UC
aseismic slip
ductile deformation
basal accretion
subducting plate
LC
Hot prism
outer ridge
forearc basin
compression
imbricate thrusts
UC
aseismic slip
basal accretion
subducting plate
LC
Cold prism

Fig. 7